Magnetic Resonance in Medicine 53:640–648 (2005)

Manganese-Enhanced Magnetic Resonance Imaging of Mouse Brain after Systemic Administration of $MnCl_2$: Dose-Dependent and Temporal Evolution of T_1 Contrast

Jung Hee Lee, Afonso C. Silva, Hellmut Merkle, and Alan P. Koretsky*

Manganese is a useful contrast agent for MRI of animals. Previously, it has been shown that systemic doses of $MnCl_2$ provide unique contrast in the rodent brain, enabling visualization of neuroarchitecture. The present work investigates the dose and temporal dependence of brain enhancement after i.v. administration of $MnCl_2$. Varying doses of $MnCl_2$ (9–175 mg/kg) were administered to mice from 0 to 24 h prior to T_1-weighted manganese-enhanced MRI (MEMRI) at 11.7 T. Pre-$MnCl_2$ T_1 values measured in different brain regions ranged from 1.17 ± 0.03 to 1.76 ± 0.01 s. Post-$MnCl_2$ T_1 measured 24 hr after administration of $MnCl_2$ were significantly decreased, even after the lowest dose of $MnCl_2$. The largest decreases occurred in the pituitary gland, where post-$MnCl_2$ T_1 ranged from 231 ± 23 ms following the lowest dose to 143 ± 43 ms after the highest dose, while the smallest decreases were observed in cortex (post-$MnCl_2$ T_1 = 1060 ± 5 ms for low dose and 637 ± 5 ms for high dose). The contrast resulting after 14 hr did not change up to 24 hr. Enhancement first occurred in subarachnoid spaces, followed by ventricles and periventricular tissues, and finally reached the remainder of the brain. Cortical layers were detected at higher doses (>88 mg/kg) and olfactory bulb layers were detected with the lowest dose (9 mg/kg). Temporal evolution of the enhancement of the olfactory bulb layers was observed. In some regions of the brain, such as hippocampus and thalamus, the changes in contrast detected between 2 and 14 hr used very specific pathways. These results demonstrate that both the dose and the time after $MnCl_2$ can be manipulated to optimize brain contrast in a region-specific manner. Published 2005 Wiley-Liss, Inc.†

Key words: MRI; contrast agents; cortical layers; hippocampus; molecular imaging

Manganese-enhanced MRI (MEMRI) is being increasingly used for MRI in animals due to the unique T_1 contrast that is sensitive to a number of biologic processes. Three specific uses of MEMRI in imaging the animal brain have been demonstrated. First, due to the fact that manganese ion (Mn^{2+}) can enter excitable cells via voltage-gated calcium channel, protocols have been devised that enable accumulation of Mn^{2+} in active areas of the brain (1–6) and heart (7,8). This technique has been referred to as activation-induced MEMRI (3,5,6). The second use of MEMRI is to trace specific neural connections in the brain. MEMRI has been shown to enable imaging anterograde connections in the olfactory (1,2), visual (1,9–11), and somatosensory pathways (12) of the rat and mouse brain after direct injection of $MnCl_2$ into a specific brain region. The song centers of the bird (13) and neural connections in the monkey (14) have also been mapped with MEMRI neuronal tracing techniques. The third use of MEMRI has been as a whole-brain contrast agent after systemic administration (4,15–17). It has been demonstrated in mice and rats that an i.p., i.v., or subcutaneous (s.c.) injection of $MnCl_2$ leads to unique MRI contrast of the brain (3,4,15–18). Taken together, MEMRI is proving useful as a new method for molecular imaging to visualize functional neural circuits and anatomy in the brain in vivo.

Various aspects of neuroarchitecture can be imaged following a systemic administration of $MnCl_2$. Dentate gyrus (DG) and CA formation of the hippocampus, layers in the olfactory bulb, cortex and cerebellum, and separation of a number of deep brain nuclei have been detected in MEMRI (4,15,17). This contrast should be very useful for quantifying various aspects of brain anatomy in vivo and is causing increased interest in understanding the mechanisms controlling the distribution of Mn^{2+} in vivo. There has been a large amount of work involved with studying the distribution of Mn^{2+} in the central nervous system, motivated in particular by two major factors. First, Mn^{2+} is an essential component of a number of key enzymes, such as glutamine synthetase and superoxide dismutase (19,20). Second, Mn^{2+} is a known neurotoxin, which, in excess in the brain, causes a disease similar to Parkinsonism (21,22). Much is known about the anatomic distribution of Mn^{2+}. Some studies have indicated that the distribution of manganese may reflect the density and/or activity of astrocytes (23), neurons (1), and mitochondria (2,19,24). However, little is known about the cellular and subcellular distribution of Mn^{2+} in the brain because of the lack of a method for histochemical staining for Mn^{2+} (25).

In addition to the spatial heterogeneity of Mn^{2+} in the brain, there is a temporal heterogeneity after systemic administration as well. The blood–brain barrier (BBB) is known to limit the rate of Mn^{2+} uptake and accumulation in the brain (3,15,17,26,27). There have been a few MRI reports on the initial pathways that Mn^{2+} takes to distribute in the brain after systemic administration in rodents (15,17). Initial uptake into choroid plexus, which then spreads to the cerebral spinal fluid (CSF) spaces in ventricles and periventricular tissues within 2 hr after administration, was observed (15). After s.c. administration the time courses of enhancement in a variety of areas of the

Laboratory of Functional and Molecular Imaging, National Institute of Neurological Disorders and Stroke, National Institutes of Health, Bethesda, Maryland.

Grant sponsor: NINDS intramural research program (Story Landis, Scientific Director).

*Correspondence to: Alan P. Koretsky, Laboratory of Functional and Molecular Imaging, National Institutes of Neurological Disorders and Stroke, 10 Center Drive, Building 10 Room B1D118, Bethesda, MD 20892-1065. E-mail: KoretskyA@ninds.nih.gov

Received 22 June 2004; revised 15 September 2004; accepted 27 September 2004.

DOI 10.1002/mrm.20368
Published online in Wiley InterScience (www.interscience.wiley.com).

brain have been reported (17). However, a detailed examination of the temporal evolution of the contrast enhancements in the brain that are usually enhanced by MEMRI has not been thoroughly investigated.

Despite the increase in interest in the contrast obtained after systemic MEMRI there has been little work addressing the dose dependence of enhancement in the rodent brain. Furthermore, there has been little work studying the changes in enhancement occurring from 2 to 24 hr after i.v. infusion of $MnCl_2$. There has been a single report describing changes in enhancement after a single dose of $MnCl_2$ (17). This work emphasized the changes in contrast that occurred in numerous brain areas, with little attention to the pathways responsible for the change in enhancement. The aim of the present work was to further characterize the effects of i.v. administration of $MnCl_2$ on T_1-weighted MEMRI of the mouse brain at 11.7 T. In particular, the effects of varying the amount of $MnCl_2$ infused were studied and the potential pathways that Mn^{2+} could take were analyzed in an attempt to help further optimize and extend systemic MEMRI techniques for visualization of neuroarchitecture.

MATERIALS AND METHODS

Animal Preparation

Experiments were carried out using 34 adult FVB mice weighting 25–28 g. An isotonic solution of $MnCl_2$ (Sigma, Aldrich, St. Louis, MO) was prepared at a concentration of 120 mM $MnCl_2$ and infused into awake mice through a tail vein line at a rate of 250 μL/hr. $MnCl_2$ infusion was followed by s.c. injection of 1 mL of normal saline solution. $MnCl_2$ was administered at six different doses: 175, 131, 88, 44, 18, and 9 mg/kg. After $MnCl_2$ infusion, the animals were returned to their cages and allowed free access to food and water. The cage was set on a heating pad overnight to aid temperature regulation of the animals. For MRI, the animals were anesthetized and set into an MR-compatible cradle. During MRI, the animals were anesthetized by breathing 2% isoflurane into oxygen-enriched air with a facemask. The rectal temperature was carefully monitored and maintained at 36 ± 1°C. MEMRI was performed 20–26 hr after $MnCl_2$ administration for all T_1 measurements, 4 animals for each dose. Two animals were used for T_1 measurements without $MnCl_2$ injected. To investigate the time course of distribution of Mn^{2+} throughout the entire brain, MEMRI was performed between 0 and 24 hr after administration of 175 mg/kg of 120 mM $MnCl_2$ solution: 3 animals during infusion and 3 animals each at 1, 2, 4, 6, 8, 10, and 24 hr after infusion.

Manganese Enhanced MRI

All MRI experiments were performed on a 11.7 T/31 cm horizontal bore magnet (Magnex Scientific, Ltd., Abbingdon, UK) interfaced to a Bruker Avance MRI console (Bruker-Biospin, Billerica, MA) equipped with a 9-cm gradient set capable of supplying up to 45 G/cm in 80 μs rise time. A second-order shim set capable of up to 4250 Hz /cm^2 was mounted outside the 9-cm gradient (Resonance Research, Billerica, MA). A 70 mm ID/89 mm OD shielded laboratory-built transmit-only birdcage coil was used for excitation and actively decoupled from a 20-mm-diameter saddle-shape surface coil, which was used for receiving the signal. High-resolution 3D MEMRI was obtained from each mouse using a spin-echo T_1-weighted MRI sequence (TR/TE = 400/6.6 ms, 100 μm isotropic resolution, FOV = 2.56 × 1.28 × 1.28 cm^3, matrix size = 256 × 128 × 128, slice selection direction = sagittal, and readout direction = head-to-foot) to evaluate the contrast.

T_1 Measurements

T_1 measurements were performed using 10 different inversion times in a standard inversion-recovery, multislice coronal T_1-weighted spin-echo sequence (TR/TE/TI = 10000/7.68/5, 10, 20, 50, 100, 200, 500, 1000, 1500, and 2000 ms, in-plane resolution: 200 × 200 μm^2, slice thickness: 500 μm). ROIs were placed in enhanced regions of pituitary gland (Pit), periventricular tissue (pv), hippocampus (HP), cortex, interpendicular nucleus (IP), cerebellum (CEB), and olfactory bulb (OB). The signal intensities of each region of interest (ROI) (700–3000 pixel units) were measured and fitted into a three-parameter function to calculate T_1 values using Bruker Paravision Software (Bruker-Biospin). T_1 (ms) ± SD were obtained by averaging four animals per dose. Two animals without $MnCl_2$ administration were subjected to T_1 measurement for baseline values.

Temporal Distribution of Manganese in the Brain

High-resolution 3D MEMRI, fast spin-echo T_1-weighted (TR/TE = 300/6.6 ms, echo train length = 2, 100 μm isotropic resolution, FOV = 2.56 × 1.28 × 1.28 cm^3, matrix size = 256 × 128 × 128, slice selection direction = sagittal, and readout direction = head to foot) were acquired with the Mn^{2+} administration of 175 mg/kg. The acquisition time for each 3D MRI data was 40 min. Relative signal intensities were normalized as a function of time by measuring the signal-to-noise ratio (SNR) in regions where significant variations in contrast were observed in time, according to the equation, SNR = 0.655 × [signal intensity/standard deviation (SD) of noise] (28) using Bruker ParaVision Software (Bruker-Biospin, Billerica, MA). The SD of the noise was measured outside the brain, but avoiding areas that might be affected. Plots of relative signal as a function of time in the graphs represent the SNR of the ROI ± SD from averaging three animals at each time point.

RESULTS

MEMRI of Mouse Brain

Figure 1 shows horizontal (left), sagittal (center), and axial (right) cuts from a typical T_1-weighted spin-echo 3D MRI of a mouse brain acquired 24 hr after i.v. infusion of 88 mg/kg of $MnCl_2$. The manganese-enhanced structures are well visualized in all 3D orientations. The horizontal sections show enhancement of the pv, the CA1, CA2, CA3, and fimbria regions of hippocampus, the arrowhead of DG, and layers of OB. In the sagittal view, the CEB shows excellent gray–white matter contrast. Other enhanced regions such as hippocampus, inferior colliculus, IP, and olfactory bulb are also shown in this view. In the coronal view, the hippocampus is enhanced with clear delineation of CA1, CA2, and CA3 regions.

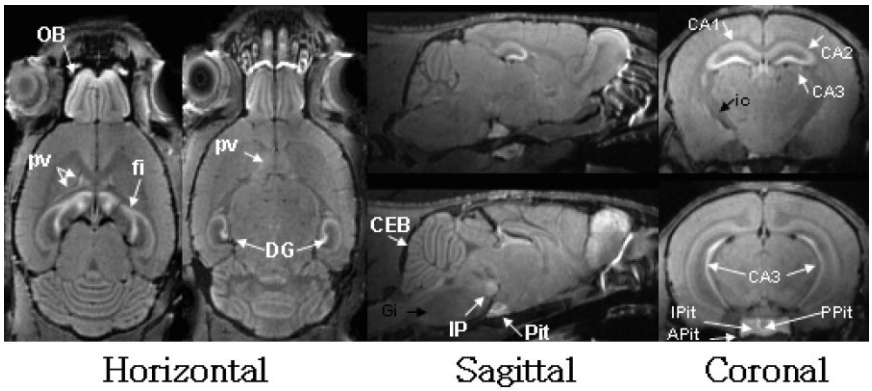

FIG. 1. Typical horizontal (left), sagittal (center), and axial (right) cuts from a T_1-weighted spin-echo 3D-MEMRI of a mouse brain acquired 24 hr after a systemic injection of 88 mg/kg of $MnCl_2$. Bright manganese-enhanced structures are well visualized in all 3D orientations. CEB: cerebellum; CA1,CA2, CA3: CA formation of hippocampus; DG: dentate gyrus; fi: fimbria of hippocampus; IP: interpeduncular nucleus; OB: olfactory bulb; APit, IPit, PPit: anterior, intermediate, and posterior lobes of pituitary gland; pv: periventricular tissue zone. The increased contrast allows clear visualization of other anatomic details of the complex brain neuroarchitecture. For example, the internal capsule (ic) and the gigantocellular reticular nucleus (Gi), appear darker than surrounding tissues in the T_1-weighted MEMRI.

The Pit is well depicted on the sagittal and coronal views, and Mn^{2+} allows clear separation of the posterior, intermediate, and anterior lobes of the Pit. Other anatomic details of the brain neuroarchitecture are evident after a systemic administration of $MnCl_2$ including the internal capsule and the gigantocellular reticular nucleus, which appear darker than surrounding tissues in T_1-weighted MEMRI. Other deep brain subnuclei of thalamus, hypothalamus, and amygdala are also more visible due to increased signal contrast (areas not labeled). The relative contrast is in good agreement with previous systemic MEMRI studies in rat and mouse (4,15,17).

Mn $^{2+}$ Dose Dependence of Regional T_1 Values

Figure 2a shows 3D MEMRI images of the mouse brain at varying doses of infused $MnCl_2$. Enhancement of the brain is clearly visible even at the lowest dose of $MnCl_2$, especially in the areas of the brain which lack a BBB, such as the Pit and the pineal gland. In addition, enhancements in pv and in OB were clearly detected at the lowest doses used. With as little as 1/10 of the maximum dose used in this study, areas such as the hippocampus, the interpeduncular nucleus, and the substructures of cerebellum were clearly enhanced. Such enhancement progressed with increasing doses of $MnCl_2$, and in general both the contrast and the SNR of the enhanced regions were increased, allowing for better delineation of subregional anatomic features, particularly within hippocampus, cortex, and deep brain nuclei.

In order to quantify the dose dependence of the MRI enhancement, T_1 maps were obtained at each of the $MnCl_2$ doses used in this study, and T_1 values across different brain regions were quantified. A significant decrease in T_1 values was noticeable in all regions at the lowest doses of $MnCl_2$ (Fig. 2b). T_1 continued to decrease with increasing doses in all regions. However, regions devoid of the BBB, such as the Pit, showed a larger decrease at the least dose and then a much slower decrease with increasing doses of $MnCl_2$. This may indicate that Mn^{2+} uptake in the Pit was limited by the ability of the pituitary to transport Mn^{2+} and not by the availability of Mn^{2+} in the blood supply or in the extravascular space surrounding the pituitary. Pre-$MnCl_2$ T_1 values in the pituitary region were 1167.0 $\pm$ 25.7 ms. This region showed the shortest T_1 values following $MnCl_2$ administration, varying from 231.0 $\pm$ 23.4 ms at the lowest dose of Mn^{2+} to 142.6 $\pm$ 42.8 ms at the highest dose of Mn^{2+}. On the other hand, the smallest effects on T_1 values by $MnCl_2$ were found in cortex, where T_1 varied from 1058.7 $\pm$ 4.5 ms at the lowest dose of $MnCl_2$ to 637.0 $\pm$ 4.9 ms at the highest dose. Pre-$MnCl_2$ T_1 in the cortex was 1570.0 $\pm$ 11.1 ms. Other brain regions had T_1 values between those found in Pit and cortex. Table 1 summarizes the dose dependence of T_1 values across different regions of the cortex.

Detection of Layers in Cortex and Olfactory Bulb

Previously, it has been shown that MEMRI can detect some of the layers in the olfactory bulb of mice and rats (4,15,17) and in the cortex of the rat (15). Figure 3 shows the appearance of cortical layers and olfactory bulb layers as a function of the amount of $MnCl_2$ infused, as indicated by the arrows. Cortical layers could be detected at doses of 88 mg/kg and above. The higher the dose of $MnCl_2$ administered, the better the contrast in the cortical layers. Olfactory bulb layers, on the other hand, could be detected even at the lowest dose tried in this study, 9 mg/kg.

Time-Course of Manganese Distribution

Figures 4–6 show 3D MEMRI of the mouse brain acquired during 0–24 hr after Mn^{2+} administration for different brain regions. Below we describe the temporal evolution of the enhancement for various brain regions.

Cerebellum (Fig. 4A and B)

Within 1 hr post-$MnCl_2$ administration the subarachnoid space surrounding the cerebellum as well as the fourth ventricle (4V) were strongly enhanced, without a signifi-

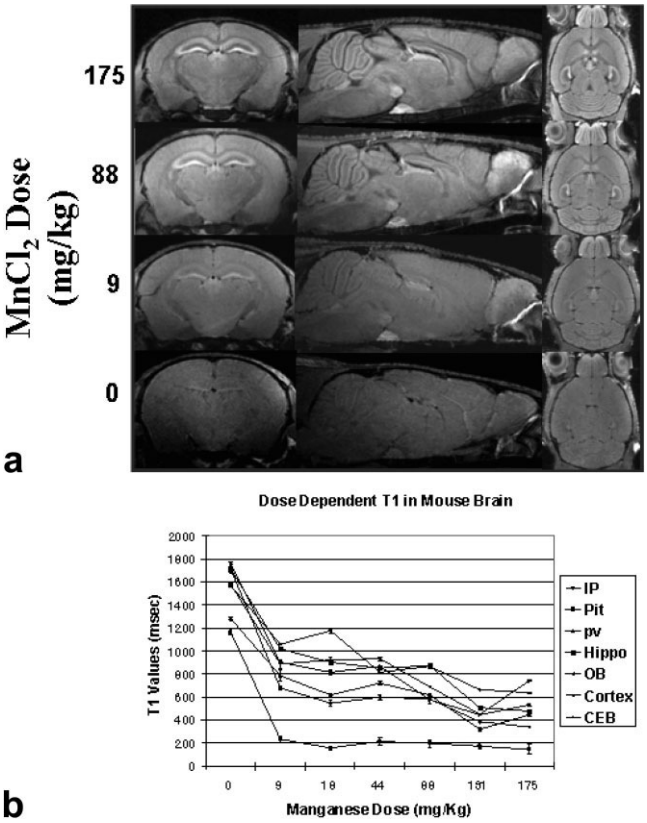

FIG. 2. Dose dependence of MEMRI contrast. (**a**) Typical horizontal (left), sagittal (middle), and coronal (right) cuts from representative 3D MEMRI are shown in each row at varying doses of $MnCl_2$. Enhancement of the brain is clearly visible even at the lowest dose of $MnCl_2$, especially in the areas of the brain devoid of the BBB, such as the pituitary and the pineal glands, in periventricular zones, and in olfactory bulb. Tissue-specific enhancement progressed with increasing doses of $MnCl_2$, and in general both the contrast and the SNR of the enhanced regions, allowing for better delineation of subregional anatomic features, particularly within hippocampus, olfactory bulb, cortex, and deep brain nuclei. Please refer to Fig. 1 for labeling of different anatomic structures. (**b**) Dose dependence of T_1 values across various regions of the mouse brain. T_1 values were obtained in the pituitary gland (Pit), periventricular tissue (pv), hippocampus (HP), cortex, interpeduncular nucleus (IP), cerebellum (CEB), and olfactory bulb (OB). A significant decrease in T_1 values was noticeable in all regions at all doses of $MnCl_2$. Regions devoid of the BBB, such as the pituitary gland, showed a dose-independent saturation in post-$MnCl_2$. For all other regions, T_1 continued to decrease with increasing doses of $MnCl_2$.

cant increase in signal from cerebellar tissue (gray matter (CGM) and white matter (CWM)), indicating that the CSF space is the major route for Mn^{2+} distribution into cerebellum. The rapid enhancement of subarachnoid space and 4V gradually decreased after 1 hr post-$MnCl_2$ administration, while CGM, CWM, and pv such as the superior medullary velum gradually enhanced and reached maximum contrast 24 hr post-$MnCl_2$ (Fig. 4B).

Olfactory bulb (Fig. 4C and D)

At 1 hr post-$MnCl_2$ administration, only the subarachnoid space surrounding the bulb showed enhancement. At 4 hr and thereafter, four layers in the olfactory bulb were visible with varying intensities in time. The olfactory nerve layer (ONL), glomerular layer (GL), external plexiform layer (EPL), and mitral cell layer (ML) could be readily distinguished. In general, the internal plexiform layer (IPL) and the granule cell layer (GrL) are better delineated in the horizontal view (Fig. 3b). The contrast proceeded from the outer ONL into the deeper layers of the bulb, causing a redistribution of enhancement until the final laminar enhancement (bright GL, ML and GrL, dark ONL, EPL, and deep layers) was achieved after 4 hr. Both the GL and the ML showed a steady increase in SNR with time. Throughout the entire time course, the GL was more prominently enhanced than ML.

Thalamus and Lateral Hypothalamic Area (Fig. 5)

Figure 5A shows a sagittal view of the mouse brain (top left). The inset images show sections of the thalamus and lateral hypothalamus before and at various times after $MnCl_2$ administration. Significant enhancement of hypothalamus commences from the pv within 1 hr of the $MnCl_2$ administration, peaks at 4 hr, and decreases progressively to lower enhancement levels. Enhancement of the thalamus occurs slowly and steadily over the 24-hr period following $MnCl_2$ administration. Figure 5B shows a plot of the temporal evolution of SNR in thalamus and lateral hypothalamus over 24 hr following $MnCl_2$ administration. The fast lateral hypothalamic enhancement precedes the steadier but slower thalamic enhancement at all times except at 24 hr post-$MnCl_2$, when the relative contrast inverts and thalamus becomes brighter than hypothalamus.

Hippocampus (Fig. 6)

Enhancement of DG, CA3, and CA2 starts as early as 1 hr post-$MnCl_2$, from the subventricular zone. Enhancement of CA1 is weakest among all other hippocampal regions. Figure 7 shows a series of consecutive 100-μm sagittal cuts from a 3D MRI data obtained 6 hr post-$MnCl_2$ administration, indicating the CA2–CA3 transition region of hippocampus. The arrows point to a region of direct contact of hippocampus with the subventricular zone. This is a major entry point for Mn^{2+} into hippocampus and indicates a specific route for $MnCl_2$ from the subventricular zone to the hippocampus.

DISCUSSION

Recently it has been shown that MRI after systemic administration of $MnCl_2$ leads to contrast sensitive to a number of features of neuroarchitecture in the rodent brain (4,15,17). In these earlier studies either a s.c. injection of a low dose (20 mg/kg) (17) or i.v., i.p., and s.c. injection of the high doses (175 mg/kg) used here were used (4,15). In the present study we showed that a wide range of systemic doses (9–175 mg/kg) leads to MRI detection of the same features described previously. Consistent with earlier studies, even at the lowest doses there was enhancement of olfactory bulb layers, the CA formation of the hippocampus, and gray matter in the cerebellum, as well as enhance-

Table 1
Dose Dependence of T_1 Values (ms) in Various Regions of the Mouse Brain

Brain region	$MnCl_2$ dose (mg/kg)						
	0	9	18	44	88	131	175
Pit	1167.0 ± 25.7	231.0 ± 23.4	154.9 ± 18.8	211.4 ± 35.6	195.4 ± 32.4	172.8 ± 25.7	142.6 ± 42.8
IP	1710.0 ± 19.7	677.3 ± 31.3	544.6 ± 34.1	599.1 ± 16.5	584.1 ± 4.31	238.8 ± 12.6	294.9 ± 8.56
pv	1280.0 ± 16.4	738.6 ± 49.2	616.2 ± 4.3	718.6 ± 17.2	615.9 ± 5.4	319.8 ± 11.4	443.4 ± 4.8
Hippo	1710.0 ± 18.2	1016.5 ± 15.1	899.8 ± 17.1	851.6 ± 6.3	870.4 ± 8.4	508.6 ± 5.5	474.7 ± 3.7
OB	1760.0 ± 11.3	899.1 ± 6.1	814.1 ± 23.3	865.5 ± 2.2	578.2 ± 5.8	447.9 ± 9.0	529.3 ± 12.7
Cortex	1570.0 ± 11.1	1058.7 ± 4.5	1174.1 ± 18.0	815.9 ± 1.7	864.1 ± 7.5	661.6 ± 3.9	637.0 ± 4.9
CEB	1580.0 ± 9.7	886.2 ± 40.1	921.1 ± 19.5	931.5 ± 14.0	690.2 ± 2.9	451.8 ± 5.1	737.5 ± 5.4

Note. A standard inversion-recovery, multislice coronal T_1-weighted spin-echo sequence with 10 inversion times (TR/TE/TI = 10000/7.68/5, 10, 20, 50, 100, 200, 500, 1000, 1500, and 2000 ms, in-plane resolution: 200×200 μm^2, slice thickness: 500 μm) was used for signal intensity measurements on ROIs that were placed in enhanced regions of pituitary gland (Pit), interpendicular nucleus (IP), periventricular tissue (pv), hippocampus (Hippo), olfactory bulb (OB), cortex, and cerebellum (CEB). The signal intensities measured at different inversion times were fitted into a three-parameter function to calculate T_1 values using Bruker Paravision Software (Bruker-Biospin). Animals were infused with 120 mM isotonic $MnCl_2$ solution at a rate of 250 μl/hr at a given dose 20–24 hr prior to T_1 measurements.

ment of numerous other regions of the brain. Also consistent with earlier studies was the detection of other features of neuroarchitecture at the highest doses of infused $MnCl_2$ such as cortical layers (4,15). Indeed, detection of cortical layers in the mouse brain became significant only above 88 mg/kg. Unfortunately it was not possible to go to higher doses of infused $MnCl_2$ due to systemic toxicity such as loss of temperature regulation. It may be possible to avoid these systemic effects and get higher levels of Mn^{2+} into the brain by direct injection into the brain or CSF space. The results clearly indicate that there is a dose dependence to some of the features of neuroarchitecture detectable by systemic MEMRI.

In the present work, we have extensively investigated the contrast enhancement profile in a wide range of Mn^{2+} doses by measuring T_1 relaxation times at various regions of the mouse brain. With increasing doses of infused $MnCl_2$ there were large decreases in mouse brain T_1 measured at 11.7 T. The changes in T_1 were heterogeneous across different regions of the brain. Some regions such as Pit dropping fast at the lowest doses and other regions such as cortex changing much slower with increasing doses of $MnCl_2$ were observed. In general the largest changes in T_1 occur by the 44–88 mg/kg doses with T_1 getting as short as 200 ms. This large shortening of T_1 explains the large degree of contrast obtained when the brain is imaged at a single TR. T_1 relaxation data were not obtained at high enough resolution to study the changes in T_1 among some of neuroarchitectural features detected, such as olfactory or cortical layers, and thus in these regions the T_1 represents an average over the heterogeneity in these tissues. Relaxation of Mn^{2+} is expected to be

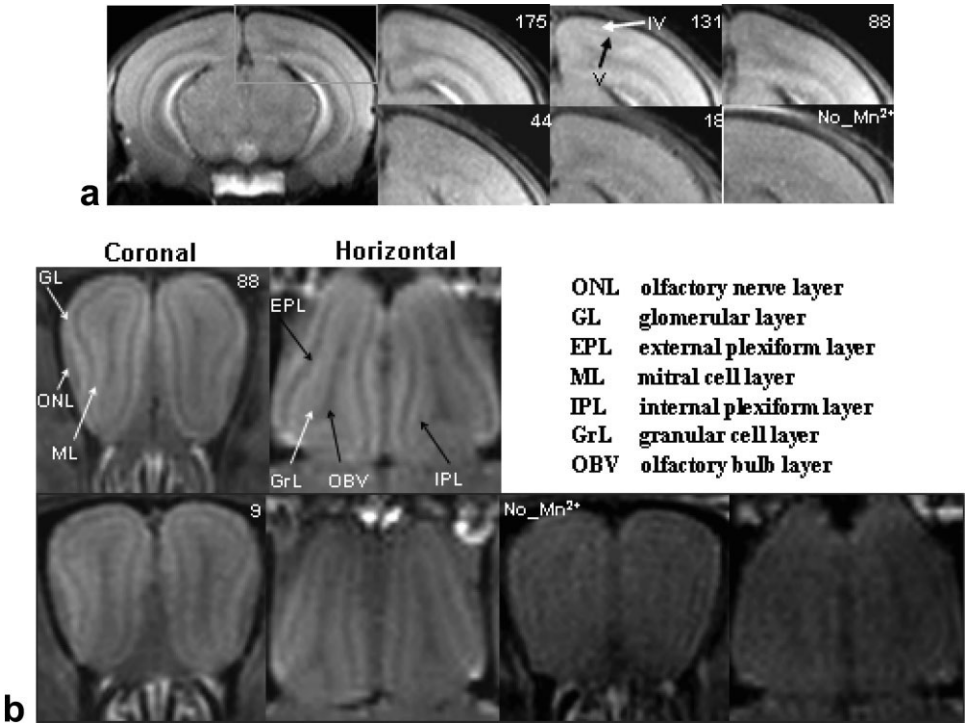

FIG. 3. MEMRI reveals brain neuroarchitecture. (**a**) Coronal section of the mouse brain (left). The inset images on the right were obtained at different $MnCl_2$ doses, indicated in each image. Cortical layers become distinguishable at doses of 88 mg/kg or greater, as indicated by the arrows. **b**) Coronal (top left) and horizontal (top right) images of the mouse olfactory bulb, showing olfactory bulb layers clearly resolved by MEMRI. Unlike cortical layers, olfactory bulb layers were well visualized even at the lowest dose of 9 mg/kg used in the present study. White arrows indicate laminae positively enhanced by $MnCl_2$, while black arrows indicate laminae that do not enhance with $MnCl_2$.

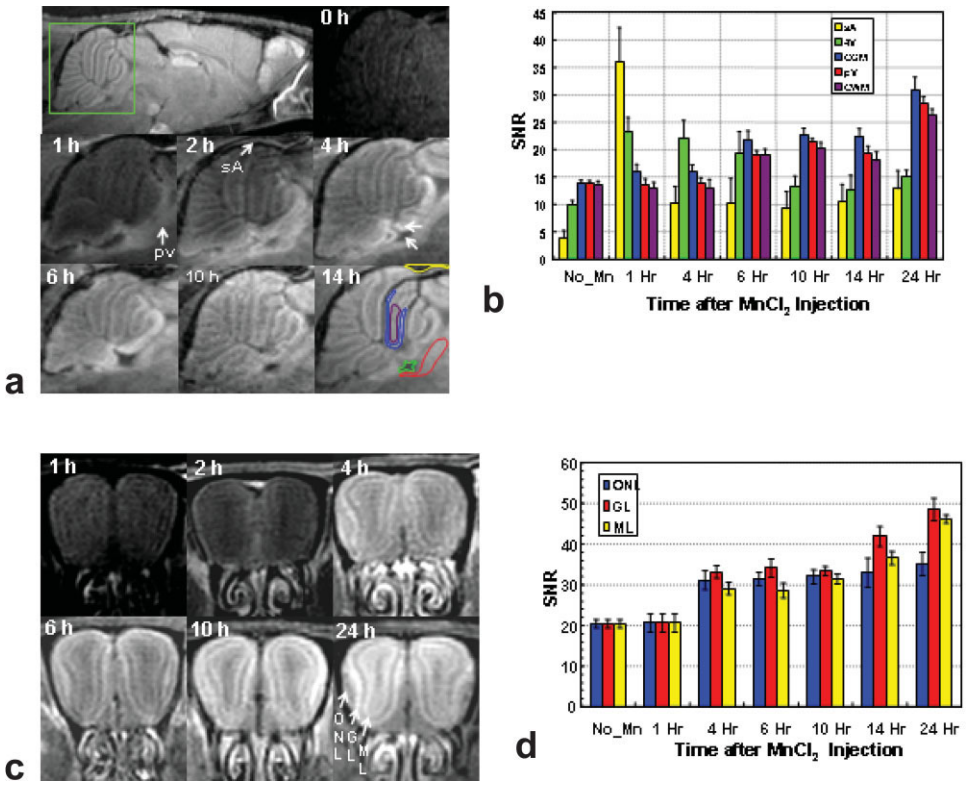

FIG. 4. The time course of signal enhancement in cerebellum and olfactory bulb. (**a**) Sagittal view (top left) of a mouse brain 24 h after $MnCl_2$ (120 mM, dose = 175 mg/kg) administration. The inset frames show the temporal evolution of signal in cerebellum before and 1 –14 h after $MnCl_2$ injection. A steady increase in signal in various regions of cerebellum is clearly visible. (**b**) A plot of the temporal evolution of SNR in five different regions of cerebellum (indicated in the 14-hr frame) shows an early enhancement of the subarachnoid space (sA) and the of the fourth ventricle (4V), followed by a steady increase of SNR in cerebellar gray matter (CGM), periventricular tissue (pv), and cerebellar white matter (CWM) with time. (**c**) Coronal images of the olfactory bulb show the temporal evolution of signal at various times after $MnCl_2$ infusion. Enhancement occurs in a layer-specific manner, with the glomerular layer (GL) showing the strongest increases. (**d**) A plot of the image SNR from ROIs placed in the olfactory nerve layer (ONL), glomerular layer (GL), and mitral cell layer (ML) show a step increase in enhancement in the ONL and a strong and gradual increase in both the GL and ML.

complicated in tissue. In addition to the amount of Mn^{2+} that accumulates in a specific brain region, its binding to cellular components, accessibility to tissue water, and the magnetic field that relaxation measurements are made are expected to affect relaxivity (29). In a previous study it was found that accumulation of approximately 10 μM Mn^{2+} in the olfactory bulb led to contrast changes similar to those detected in this study, indicating that low levels of Mn^{2+} are responsible for the changes in T_1 that were measured in this study (2). In future studies it will be interesting to quantitate total manganese levels in different brain regions to see whether the differences in enhancements are due to differences in accumulation of Mn^{2+}, differences in relaxivity or a combination.

The time-course of redistribution of contrast in the period from 0 to 14 hr after i.v. administration varied across different regions of the brain. It was demonstrated that most of the Mn^{2+} enters the brain through the choroid plexus into CSF spaces during the initial 2 hr (15). As shown for cerebellum and olfactory bulb in Fig. 4, the subarachnoid space filled with CSF at the initial stages, e.g., 1–4 hr after Mn^{2+} injection, and then the enhancement spreads into the enhanced spaces in the tissues with time. Contrast seemed to flow into the cortex from subarachnoid spaces at the surface of the brain. Occasionally enhancement tended to flow radially into the cortex along what appeared to be veins (data not shown). This observation suggests that the distribution of Mn^{2+} may use paravascular spaces surrounding large penetrating vessels to permeate some regions of the brain (30,31). The entire cerebellum seems to be enhanced in time. The signal intensities measured in various locations within the cerebellum increased in time at similar rates, indicating that Mn^{2+} is transported into cerebellum via surrounding CSF carrying Mn^{2+}, which appears to be the major route for Mn^{2+} distribution into cerebellum.

The distribution of enhancement for olfactory bulb after systemic injection of $MnCl_2$ suggests that the full range of mechanisms are used for Mn^{2+} to enter the brain tissues. The CSF in the subarachnoid space enhanced earliest, as did inputs from turbinates into the ONL. Enhancement could be readily detected in turbinates, indicating that a source of Mn^{2+} into the ONL is from olfactory neurons (Fig. 4C). Finally, tracks of enhancement could be seen leading to or from the olfactory bulb and from cortex as well as from deep brain regions. Previously it has been shown that Mn^{2+} placed in the nose will track into the olfactory bulb via the ONL (2) and that Mn^{2+} can leave the

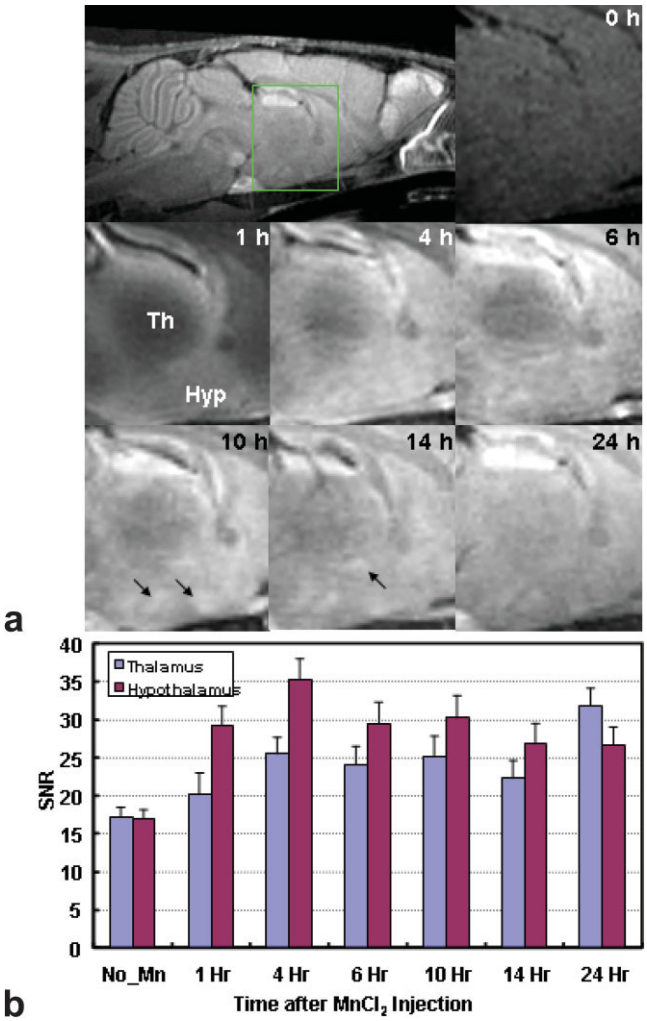

FIG. 5. The time course of signal enhancement in the thalamus and lateral hypothalamic area after $MnCl_2$ (120 mM, dose = 175 mg/kg) administration. (**a**) Sagittal view of the mouse brain (top left). The inset images show sections of the thalamus and hypothalamus before and at various times after $MnCl_2$ administration. (**b**) Significant enhancement of hypothalamus commences within 1 hr of the $MnCl_2$ administration, peaks at 4 hr, and decreases progressively to lower enhancement levels. Thalamic enhancement, however, occurs slowly and steadily over the 24-hr period following $MnCl_2$ administration.

olfactory bulb and enter pyriform cortex (1). At the temporal resolution used in this study, it was not possible to determine whether contrast was entering or leaving the bulb along these paths.

The lateral hypothalamic area showed a very interesting enhancement pattern between 4 and 6 hr after injection. The interesting finding in the lateral thalamic area during this period was that there were enhanced, discrete regions (arrows in Fig. 5A) throughout the entire lateral hypothalamic area. Enhancement in this area entered from nearby CSF in the third ventricle. The contrast defining the areas disappeared after 14 hr, due to an increase in intensity throughout the hypothalamus. Mn^{2+} has been shown to enter brain areas associated with increased activity (1–3,5,7,17,23). It is interesting to speculate that the enhancement in specific regions of the hypothalamus are associated with increased activity in specific hypothalamic nuclei as Mn^{2+} enters from CSF. Recently it has been shown in mouse auditory cortex that constant exposure to noise after systemic administration of Mn^{2+} leads to specific enhancement in the auditory cortex (32). This result indicates that activity may modulate the uptake into specific brain regions after systemic administration of Mn^{2+}. Another possibility is that the discrete spots detected represent fibers of the medial forebrain bundle present in lateral hypothalamus, which are enhanced as Mn^{2+} moves to its final distribution in the brain.

Perhaps the region of the brain that showed the most specific pathway of change in contrast was the hippocampus. The hippocampus consists of CA1, CA2, and CA3 regions and DG. Information is known to flow across the perforant pathway that connects subiculum to DG. The DG neurons in turn send axons to CA3 via mossy fibers that subsequently transmit axons to CA1 via Schaeffer collat-

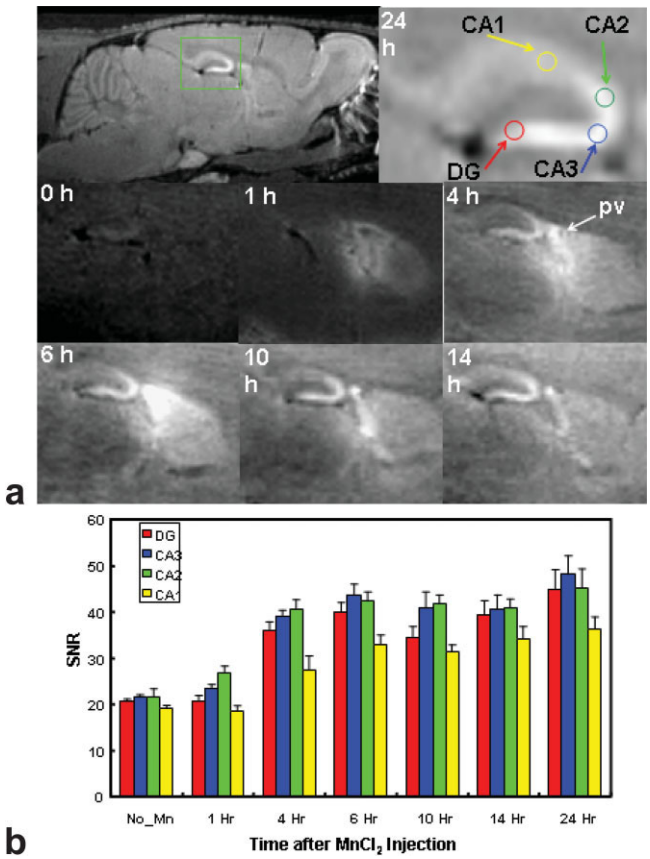

FIG. 6. The time course of signal enhancement in hippocampus after $MnCl_2$ (120 mM, dose = 175 mg/kg) administration. (**a**) Sagital view of the mouse brain. The inset images show the evolution of enhancement at several times following $MnCl_2$ administration. Enhancement of dentage gyrus (DG), CA3, and CA2 starts as early as 1 hr post-$MnCl_2$, by diffusion of Mn^{2+} from the periventricular zone (pv) surrounding the lateral ventricles. By 6 hr post-$MnCl_2$, contrast is maximized. Enhancement of CA1 is significantly smaller than those of the other three hippocampal regions. (**b**) A plot of the time course over DG, CA3, CA2, and CA1 obtained from the ROIs indicated at the top right of (A). Contrast for all regions reaches final levels at 6 hr post-$MnCl_2$ administration.

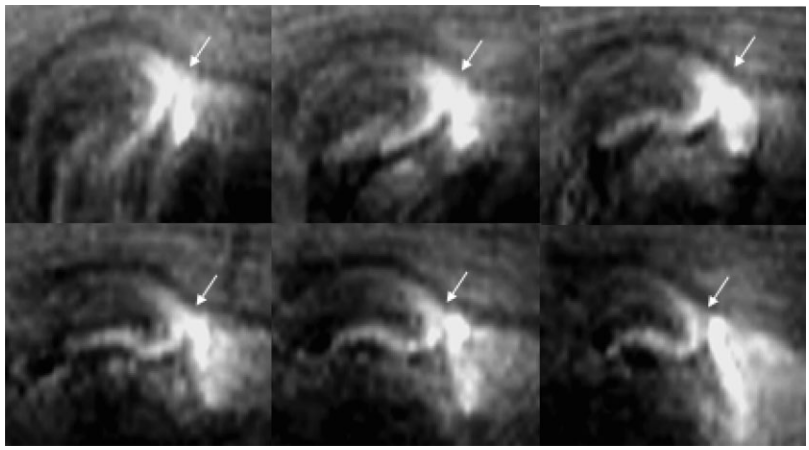

FIG. 7. A series of consecutive 100-μm sagittal cuts from a 3D MRI data obtained 6 hr after $MnCl_2$ (120 mM, dose = 175 mg/kg) administration, showing the CA2–CA3 transition region of hippocampus. The arrows indicate a direct contact of hippocampus with the subventricular zone (SVZ) surrounding the lateral ventricles, which is the probable entry point for Mn^{2+} into hippocampus.

erals. In our 3D MRI data, the CA2–CA3 region of the hippocampus showed a close contact with a specific region of the ventricle starting sometime between 1 and 4 hr after injection. The contact distance was about 500–600 μm in distance (Fig. 7). Therefore, Mn^{2+} present in the subventricular zone (SVZ) was transported into hippocampus through the contact with the CA2–CA3 regions of hippocampus. Thereafter, enhancement moved from the CA2–CA3 regions to the CA1 region and DG of the hippocampus. The CA2–CA3 regions of the hippocampus showed a higher intensity throughout the time course of enhancement, which may be due to the direct supply of Mn^{2+} from CSF at the contact point with SVZ.

The fact that systemic MEMRI leads to the ability to measure a number of features of neuroarchitecture makes it important to understand the mechanisms responsible for the final enhancements achieved. This is a challenging problem because it is clear that many factors can affect the final distribution and relaxivity of Mn^{2+}. As described above, the specific path of entry from blood into different regions of the brain vary depending on permeability of blood vessels, proximity to ventricles, and potentially the density of projections that can carry Mn^{2+} *via* peripheral neurons. There are also a number of mechanisms that can transport Mn^{2+} (33–40), a number of cellular structures such as proteins (e.g., calcium binding proteins) that can bind Mn^{2+}, and organells (e.g., mitochodria) that have different affinity for Mn^{2+} (19,20,24). The regional cell density and activity should also affect the amount of uptake into specific regions of the brain (1–3,5,7,17,23). At the current state of knowledge, the exact mechanisms of Mn^{2+} distribution in the brain and the quantitative distribution in different brain regions after systemic administration of $MnCl_2$ are not well described. The results of the current work should give some insights for further investigation of the mechanisms of Mn^{2+} distribution in the brain.

In conclusion, the results of the current study demonstrate that there is a dose and temporal dependence to the contrast that can be achieved with systemic MEMRI. The optimal dose of Mn^{2+} and the time that MRI is performed after a systemic dose of Mn^{2+} should be determined depending on the target region of investigation for achieving maximum contrast enhancement. In addition, given the dose-dependent decrease in T_1, MRI acquisition parameters can be adjusted according to the dose of Mn^{2+} administered. Systemic MEMRI should be useful for studying neuroarchitectural changes under a number of conditions including studying brain development and changes in brain anatomy associated with neurologic diseases. If specific processes can be determined to control the enhancement detected after systemic MEMRI, this will open the door to using systemic Mn^{2+} as an MRI contrast technique for molecular imaging of those processes.

ACKNOWLEDGMENTS

The authors acknowledge Ms. Torri Wilson for the excellent technical assistance of animal preparation and Dr. Kai-Hsiang Chuang for helping with image processing.

REFERENCES

1. Pautler RG, Silva AC, Koretsky AP. In vivo neuronal tract tracing using manganese-enhanced magnetic resonance imaging. Magn Reson Med 1998;40:740–748.
2. Pautler RG, Koretsky AP. Tracing odor-induced activation in the olfactory bulbs of mice using manganese-enhanced magnetic resonance imaging. Neuroimage 2002;16:441–448.
3. Lin YJ, Koretsky AP. Manganese ion enhances T1-weighted MRI during brain activation: an approach to direct imaging of brain function. Magn Reson Med 1997;38:378–388.
4. Lin YJ. MRI of the rat and mouse brain after systemic administration of MnCl2. Ph.D. Dissertation, Carnegie Mellon University, Pittsburg, PA. 1997; 149 p.
5. Duong TQ, Silva AC, Lee SP, Kim SG. Functional MRI of calcium-dependent synaptic activity: cross correlation with CBF and BOLD measurements. Magn Reson Med 2000;43:383–392.
6. Aoki I, Tanaka C, Takegami T, et al. Dynamic activity-induced manganese-dependent contrast magnetic resonance imaging (DAIM MRI). Magn Reson Med 2002;48:927–933.
7. Hu TC, Pautler RG, MacGowan GA, Koretsky AP. Manganese-enhanced MRI of mouse heart during changes in inotropy. Magn Reson Med 2001;46:884–890.
8. Krombach GA, Saeed M, Higgins CB, Novikov V, Wendland MF. Contrast-enhanced MR delineation of stunned myocardium with administration of MnCl(2) in rats. Radiology 2004;230:183–190.
9. Lin CP, Tseng WY, Cheng HC, Chen JH. Validation of diffusion tensor magnetic resonance axonal fiber imaging with registered manganese-enhanced optic tracts. Neuroimage 2001;14:1035–1047.
10. Ryu S, Brown SL, Kolozsvary A, Ewing JR, Kim JH. Noninvasive detection of radiation-induced optic neuropathy by manganese-enhanced MRI. Radiat Res 2002;157:500–505.

11. Watanabe T, Michaelis T, Frahm J. Mapping of retinal projections in the living rat using high-resolution 3D gradient-echo MRI with Mn2+-induced contrast. Magn Reson Med 2001;46:424–429.
12. Allegrini PR, Wiessner C. Three-dimensional MRI of cerebral projections in rat brain in vivo after intracortical injection of MnCl2. NMR Biomed 2003;16:252–256.
13. Van der LA, Verhoye M, Van MV, et al. In vivo manganese-enhanced magnetic resonance imaging reveals connections and functional properties of the songbird vocal control system. Neuroscience 2002;112: 467–474
14. Saleem KS, Pauls JM, Augath M, et al. Magnetic resonance imaging of neuronal connections in the macaque monkey. Neuron 2002;34:685–700.
15. Aoki I, Wu YJ, Silva AC, Lynch RM, Koretsky AP. In vivo detection of neuroarchitecture in the rodent brain using manganese-enhanced MRI. Neuroimage 2004;22:1046–1059.
16. Natt O, Watanabe T, Boretius S, Radulovic J, Frahm J, Michaelis T. High-resolution 3D MRI of mouse brain reveals small cerebral structures in vivo. J Neurosci Methods 2002;120:203–209.
17. Watanabe T, Natt O, Boretius S, Frahm J, Michaelis T. In vivo 3D MRI staining of mouse brain after subcutaneous application of MnCl2. Magn Reson Med 2002;48:852–859.
18. Lauterbur PC. NMR imaging in biomedicine. Cell Biophys 1986;9:211–214.
19. Akai F, Maeda M, Suzuki K, Inagaki S, Takagi H, Taniguchi N. Immunocytochemical localization of manganese superoxide dismutase (Mn-SOD) in the hippocampus of the rat. Neurosci Lett 1990;115:19–23.
20. Wedler FC, Denman RB. Glutamine synthetase: the major Mn(II) enzyme in mammalian brain. Curr Top Cell Regul 1984;24:153–169.
21. Aschner M. Manganese: brain transport and emerging research needs. Environ Health Perspect 2000;108:429–432.
22. Pal PK, Samii A, Calne DB. Manganese neurotoxicity: a review of clinical features, imaging and pathology. Neurotoxicology 1999;20: 227–238.
23. Henriksson J, Tjalve H. Manganese taken up into the CNS via the olfactory pathway in rats affects astrocytes. Toxicol Sci 2000;55:392–398.
24. Gavin CE, Gunter KK, Gunter TE. Manganese and calcium efflux kinetics in brain mitochondria. Relevance to manganese toxicity. Biochem J 1990;266:329–334.
25. Malecki EA, Devenyi AG, Beard JL, Connor JR. Existing and emerging mechanisms for transport of iron and manganese to the brain. J Neurosci Res 1999;56:113–122.
26. Murphy FB, Fernandez MP, Kossoff MB, Dillehay DL, Malko JA, Bernardino ME. Direct hepatic tumor injection in rats: can it be used for analysis of MR imaging contrast agent? J Magn Reson Imaging 1991;1: 83–85.
27. Rabin O, Hegedus L, Bourre JM, Smith QR. Rapid brain uptake of manganese(II) across the blood-brain barrier. J Neurochem 1993;61: 509–517.
28. Firbank MJ, Coulthard A, Harrison RM, Williams ED. A comparison of two methods for measuring the signal to noise ratio on MR images. Phys Med Biol 1999;44:N261–N264.
29. Kang YS, Gore JC, Armitage IM. Studies of factors affecting the design of NMR contrast agents: manganese in blood as a model system. Magn Reson Med 1984;1:396–409.
30. Rennels ML, Gregory TF, Blaumanis OR, Fujimoto K, Grady PA. Evidence for a 'paravascular' fluid circulation in the mammalian central nervous system, provided by the rapid distribution of tracer protein throughout the brain from the subarachnoid space. Brain Res 1985;326: 47–63.
31. Rennels ML, Blaumanis OR, Grady PA. Rapid solute transport throughout the brain via paravascular fluid pathways. Adv Neurol 1990;52: 431–439.
32. Yu X, Wadghiri YJ, Sanes D, Thrnbull D. Mn-Enhanced MRI (MEMRI) of auditory brain activity in unilaterally deafened mice. Proceedings of the 12th Annual Meeting of the ISMRM, Kyoto, Japan, 2004. p 639. Ref Type: Abstract
33. Frame MD, Milanick MA. Mn and Cd transport by the Na-Ca exchanger of ferret red blood cells. Am J Physiol 1991;261:C467–C475.
34. Grabill C, Silva AC, Smith SS, Koretsky AP, Rouault TA. MRI detection of ferritin iron overload and associated neuronal pathology in iron regulatory protein-2 knockout mice. Brain Res 2003;971:95–106.
35. Gunshin H, Mackenzie B, Berger UV, et al. Cloning and characterization of a mammalian proton-coupled metal-ion transporter. Nature 1997;388:482–488.
36. Gunshin H, Allerson CR, Polycarpou-Schwarz M, et al. Iron-dependent regulation of the divalent metal ion transporter. FEBS Lett 2001;509: 309–316.
37. Gunther T, Vormann J, Cragoe EJ, Jr. Species-specific Mn2+/Mg2+ antiport from Mg2(+)-loaded erythrocytes. FEBS Lett 1990;261:47–51.
38. Narita K, Kawasaki F, Kita H. Mn and Mg influxes through Ca channels of motor nerve terminals are prevented by verapamil in frogs. Brain Res 1990;510:289–295.
39. Nordhoy W, Anthonsen HW, Bruvold M, Jynge P, Krane J, Brurok H. Manganese ions as intracellular contrast agents: proton relaxation and calcium interactions in rat myocardium. NMR Biomed 2003;16:82–95.
40. Sotogaku N, Oku N, Takeda A. Manganese concentration in mouse brain after intravenous injection. J Neurosci Res 2000;61:350–356.